Journal of Nuclear Materials 404 (2010) 222–230

Contents lists available at ScienceDirect

Journal of Nuclear Materials

journal homepage: www.elsevier.com/locate/jnucmat

Deformed microstructures of two-phase Zr–2.5Nb alloy: Effects of the second phase hardness

S.K. Sahoo [a], V.D. Hiwarkar [a], L. Jain [a], I. Samajdar [a,*], P. Pant [a], G.K. Dey [b], D. Srivastav [b], R. Tewari [b], S. Banerjee [b]

[a] Department of Metallurgical Engineering and Materials Science, Indian Institute of Technology Bombay, Mumbai, India
[b] Materials Science Division, Bhabha Atomic Research Center, Mumbai, India

ARTICLE INFO

Article history:
Received 7 January 2010
Accepted 20 July 2010

ABSTRACT

Two types, A and B, of Zr–2.5Nb samples were subjected to compression tests. Both samples consisted of similar microstructure – hexagonal closed packed (hcp) α phase (the primary phase) and grain boundary bcc (body centered cubic) β phase. However, the hardness of the β phase differed between the samples – respectively being hard (sample A) and soft (sample B) relative to the primary phase. This difference was caused by the presence of fine ω precipitates. The relative hardness of β phase determined almost all aspects of deformed microstructure developments. In sample A, the primary phase had higher lattice strain and in-grain misorientation developments. In sample B, on the other hand, the softer β phase was clearly linked to more deformation twinning and associated grain size refinement and 'texturing' of the hcp α phase.

1. Introduction

Plastic deformation in multi-phase systems is a subject of both scientific and applied interests [1–10]. The mechanical properties of the second phase can have strong influence on the deformation induced microstructural developments of the primary phase [1–10]. This can be illustrated easily with the following examples. The hard and non-shearable constituent particles in a commercial aluminum alloy can create the so-called particle deformed zones in the matrix phase [2,11–14]. Presence of shearable or semi-shearable second phase, on the other hand, is expected to accommodate at least part of the strain of the primary phase [10,15]. However, such observations [1–15] are/were always made in different systems or alloys. If one can have two ideal systems, with nearly identical two-phase structures but different hardness(es) for the constituent phases – then that can indeed be a model alloy for interesting experimental studies on plastic deformation. And this formulates the motivation behind the present study.

Two phase Zr–2.5Nb can be an ideal system for 'tailored' studies on phase transformation and plastic deformation [10,15–25]. The classical two-phase microstructure of Zr–2.5Nb pressure tube [26–28] consists of hcp (hexagonal closed packed) α grains and near continuous filaments of bcc (body centered cubic) β [10,25,29]. The β size and morphology can be controlled significantly through heat-treatments [29,30]. The β is expected to be soft [10,25], though literature [31] does present us with possibilities on hard β as well. Formation of martensite and/or ω precipitates [16–25] may explain such hard β.

In the present study, cold rolled Zr–2.5Nb was given suitable heat-treatments [30]. The aim was to obtain nearly identical microstructures, hcp α with grain boundary bcc β, but microstructures with hard and soft β respectively. This was achieved through presence and absence of fine ω precipitates, which made the second phase hard or soft with respect to the primary phase. These two structures were then subjected to compression tests: objective was to monitor and comprehend the microstructural developments.

2. Experimental details

2.1. Material and sample preparation

Cast Zr–2.5Nb alloy, with chemical composition of Nb: 2.51 wt.%, O: 1092 ppm, Fe: 1250 ppm, H: <10 ppm and N: 30 ppm, was subjected to 50% reduction by cold rolling. This was done in a laboratory rolling mill in five passes: approximately 10% reduction in each pass. Cylindrical compression specimens were then machined from the rolled plate(s) – see Fig. 1. These were then heat treated at 700 °C for 14 days followed by air cooling and furnace cooling. These samples were generically termed as sample A and sample B respectively. Both samples showed hcp α phase and grain boundary β phase. Though there were differences in α/β grain size/shape (Figs. 2a and 3), the important difference

* Corresponding author. Tel.: +91 2225767621; fax: +91 2225723480.
E-mail address: indra@iitb.ac.in (I. Samajdar).

0022-3115/$ - see front matter © 2010 Elsevier B.V. All rights reserved.
doi:10.1016/j.jnucmat.2010.07.028

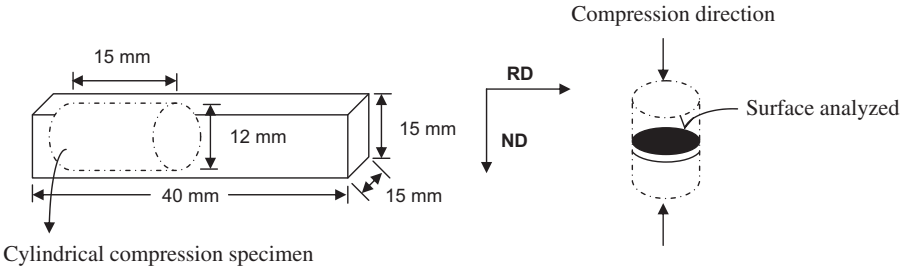

Fig. 1. Schematic showing dimensions and orientation of cylindrical compression specimens and the parent rolled plate.

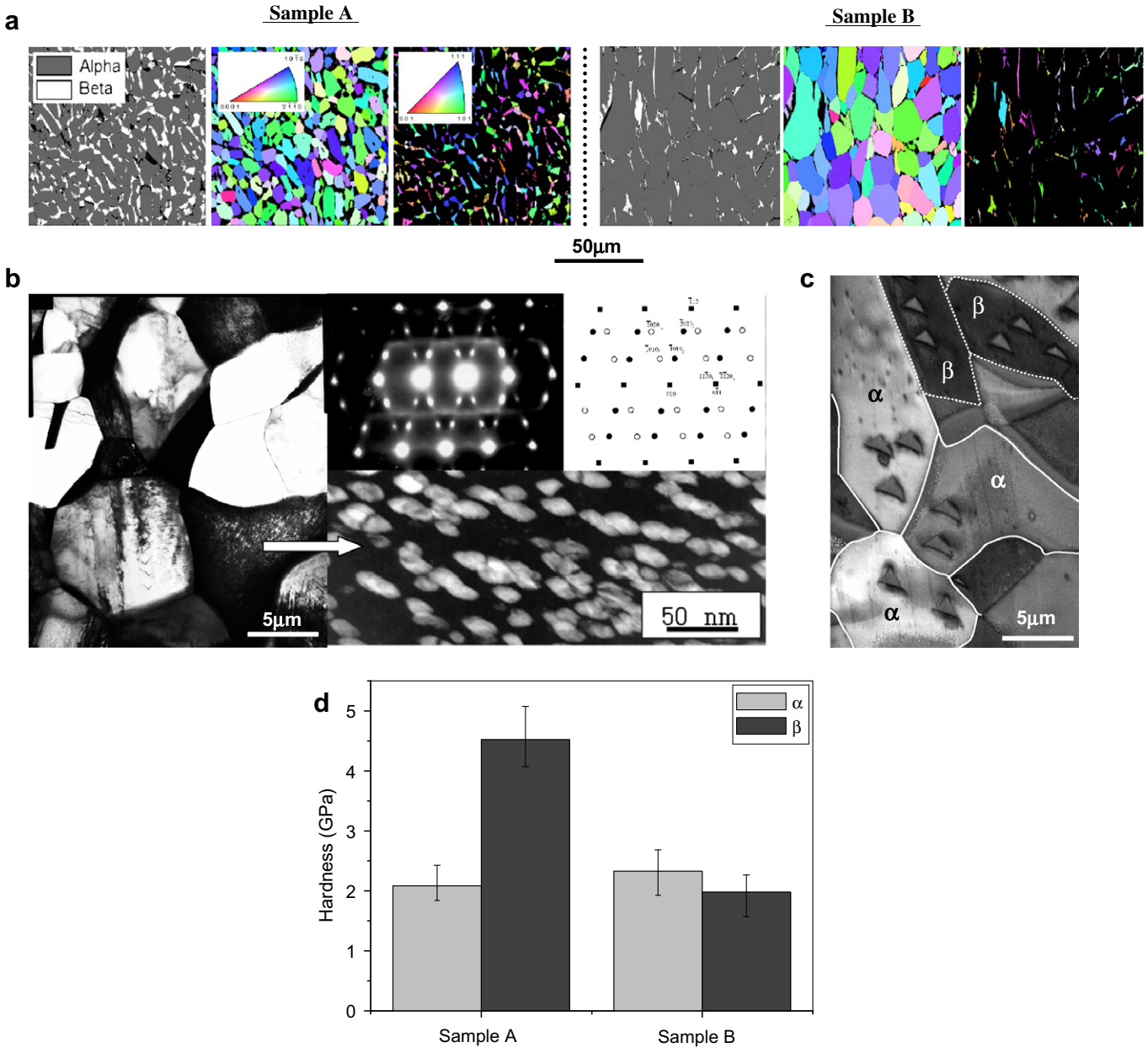

Fig. 2. (a) Starting microstructures of samples A and B. Included are phase maps and IPF (inverse pole figure) maps. The later represented α and β phases respectively. The dark regions, in the respective IPFs, represent the 'other' phase (e.g. β in α-IPF and α in β-IPF). (b) TEM microstructure of sample A, showing visible presence of ω phase in β. This was confirmed through higher magnification imaging and also electron diffraction. ω was not observed in the β of sample B. (c) Image quality (IQ) map of sample A after nanoindentation. (d) Nano-hardness of both α and β phases in samples A and B. Error bars represent the standard deviations estimated from multiple hardness measurements.

between the two samples was in the relative hardness of the β phase – see Fig. 2c and d. Such differences in microstructures and hardness are described in further details at the beginning of the 'results'.

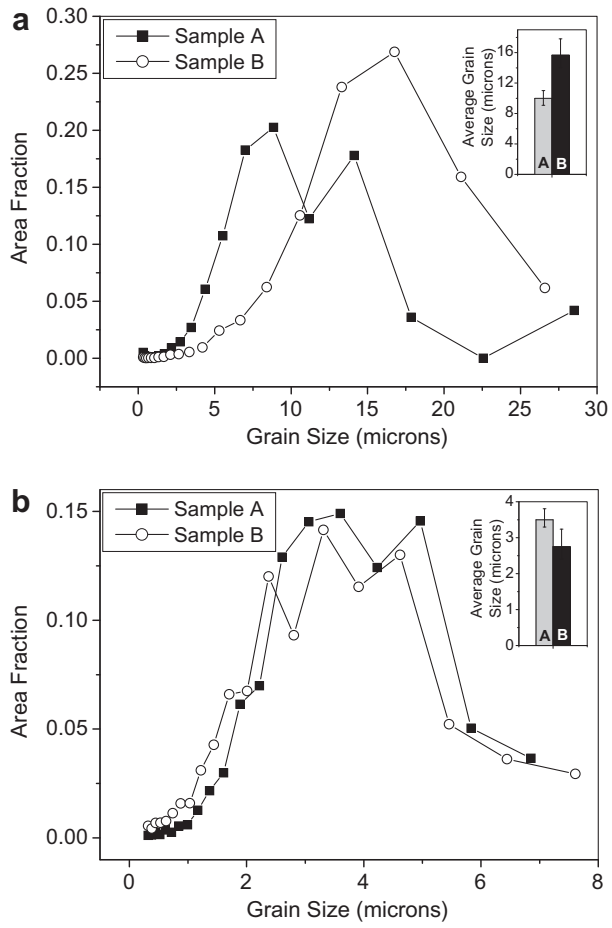

Fig. 3. Grain size distribution of (a) α and (b) β phases of the starting structures of sample A and sample B. Inserts show the average grain sizes – error bars indicating standard deviations estimated from multiple EBSD scans.

Both the specimens were subjected to 'controlled' uniaxial cold compression in a servo-hydraulic mechanical testing system (MTS) machine. Reductions of 4.5%, 13% and 37% for sample A, and of 5.5%, 11% and 31% for sample B, were given. The slight differences in reductions, between the samples, were not by design. It was caused by machine limitations in reproducing identical reductions in both samples. As shown in Fig. 1, mid-thickness sections of the respective compression planes were used for subsequent characterizations. For that purpose, the samples were electropolished using an electrolyte of 80:20 (volume percentage) of methyl alcohol and perchloric acid under 21 V at −40 °C.

2.2. X-ray diffraction (Xrd)

Bulk texture and lattice strain measurements were performed using X-ray diffraction. A Panalytical MRD system was used. It needs to be noted that during progressive deformations, β phases/grains could not be effectively resolved in Xrd. This was valid for higher strains, possibly because of a combination of grain size refinement and defect accumulation. The Xrd measurements were hence restricted to the α phase.

For bulk crystallographic texture, five pole figures ((0 0 0 2), $(01\bar{1}0)$, $(01\bar{1}1)$, $(11\bar{2}0)$ and $(01\bar{1}2)$) of α phase were measured. Subsequent texture analyses were conducted through a commercial program LaboTex [32]. As the compression tests were axi-symmetric, inverse pole figures (IPF) [33,34] were used for texture representation.

Lattice strains were estimated from X-ray peak broadening i.e. FWHM (full width half maximum) values – from the slopes of Sinθ vs. BCosθ [35–37]. Where,

$$B^2 = B_r^2 - B_a^2 \quad (1)$$

B_r and B_a are the full width half maximum (FWHM) of different (hkil) planes of the deformed and undeformed specimens respectively and θ is the Bragg angle. The Williamson-Hall treatment [35–37] separates effects of lattice strain and size: slope represent strain, while y-axis intercept may be used for size.

2.3. Nanoindentation

Nanoindentation was carried out using a Hysitron Triboindenter (TI 900). A Berkovich diamond indenter was used for the indentation. About 10 grains of both α and β phases were indented in each sample. The nano-hardness H_n is defined as [38,39],

$$H_n = P_{max}/A_c \quad (2)$$

where P_{max} is the maximum indentation load and A_c is the projected contact area at the peak load. In the present study the maximum indentation load for α and β grains/regions was 4000 and 7000 μN respectively. This was based on initial trials of varying loads and estimations based on projected area of indentation [38,39].

2.4. Electron backscattered diffraction (EBSD)

The EBSD measurements were taken on FEI Quanta-3D-FEG scanning electron microscope using a TSL-OIM (Tex. SEM Ltd. – Orientation Imaging Microscopy) EBSD package. In each sample, an approximate area of 1 mm × 1 mm was scanned by the EBSD. Beam and video conditions were kept identical between the scans and a step size of 0.2 μm was used.

In EBSD analyses, grains were identified based on 15° misorientation criterion - i.e. continuous presence of more than 15° boundary (including the twin boundaries) demarcated the grains for further data processing. Twin boundaries were identified through appropriate axis angle relationship, 94.8°. $\langle 12\bar{1}0\rangle$ for $\{10\bar{1}2\}$ $\langle\bar{1}011\rangle$ tensile twins in hcp Zr [40,41]. These were the only twins observed in the present study. Phase maps, image quality (IQ) and inverse pole figure (IPF) maps were used for microstructural representations [42]. EBSD data were also analyzed to bring out trends in-grain size, twin fraction and GAM (grain average misorientation) developments. GAM provides average misorientation between neighboring measurement points in a grain.

2.5. Transmission electron microscopy (TEM)

A JEOL 3010 TEM (300 kV operating voltage) was used for the TEM investigations. TEM was used to bring out the relative presence/absence of ω phase.

3. Results

Figs. 2 and 3 show details of the starting microstructures of samples A and B. As shown in the figures, the microstructural differences, between the samples, can be generalized in terms of differences in-grain size and shape and also in the relative hardness of the second phase. For example,

- Though the shape of α was nearly identical between the samples, α grains were larger (approximately 1.5 times) in sample B, see Figs. 2a and 3a.

- β grains were slightly smaller, but more elongated, in sample B, see Figs. 2a and 3b.
- β in sample B was softer than α, while the reverse was true for sample A, see Fig. 2c and d. Presence of ω precipitates (Fig. 2b) was responsible for significantly harder (Fig. 2d) β in sample A.

The deformed microstructures, as shown in Fig. 4, were visibly different between samples A and B. The figure shows, albeit qualitatively, that harder β in sample A was less affected than the softer β of sample B. This difference was further explored/quantified in terms of grain size refinement and deformation twinning, deformation texture developments and signatures of relative

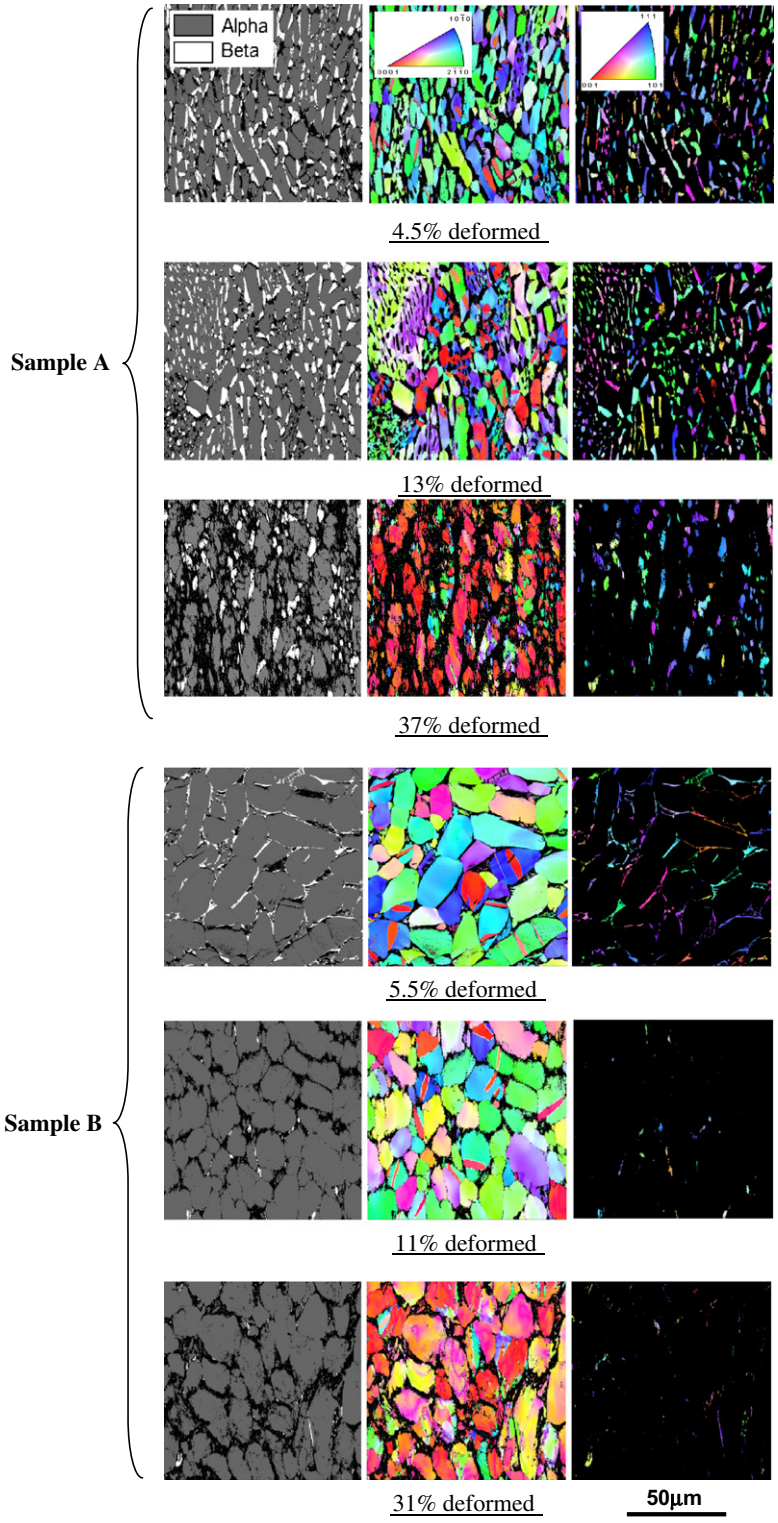

Fig. 4. Phase and IPF (for both α and β) maps of samples A and B after different deformations. The dark regions, in the respective IPFs, represent the 'other' phase (e.g. β in α-IPF and α in β-IPF) plus the non-indexed points – especially valid for β in deformed sample B.

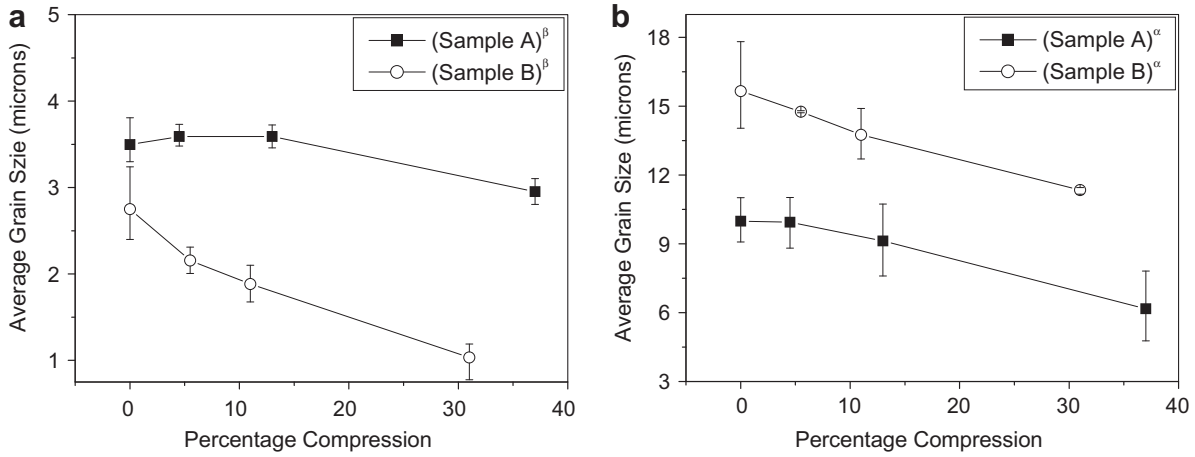

Fig. 5. Average grain size of (a) β and (b) α at different deformations for samples A and B. Error bars represent the standard deviations estimated from multiple EBSD scans.

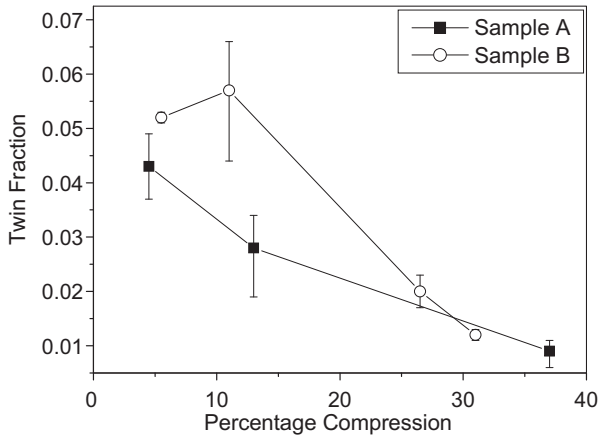

Fig. 6. Estimated twin fractions (frequency or number fractions) in α phase after different deformations. Error bars represent the standard deviations estimated from multiple EBSD scans. Twin fraction for an intermediate deformation percentage (26.5%) in sample B has also been incorporated. This was to validate that twin fractions in α of sample B remained higher, than sample A, even at the later stages of plastic deformation.

deformation. The latter was in terms of developments in lattice strain, nano-hardness and GAM values.

3.1. Grain size refinement and deformation twinning

Plastic deformation can refine the grain size through creation of new grain boundaries – new lattice curvatures created through geometrically necessary dislocations [2,15,43,44] and deformation twinning [15,45–48]. Refinement in-grain size is collated in Fig. 5 for both α and β phases, while the estimated twin fractions are plotted in Fig. 6. As shown in Fig. 5a, the refinement of the harder β (β phase in sample A) was significantly less. However, α grain size refinement in sample A was also less – at least during the initial stages of plastic deformation, see Fig. 5b. This apparent contradiction, that softer α in sample A had lesser grain size refinement, is clearly related to deformation twinning – Fig. 6. The higher deformation twinning in the α phase of sample B was responsible for more significant grain size refinement.

3.2. Developments in deformation texture

Deformation texture developments in α and β phases are captured through inverse pole figures in Figs. 7 and 8. It is to be noted that the texture measurements in the primary α was done through X-ray diffraction, while measurements for second phase β was through EBSD. α texture development showed clear patterns of increase in basal orientations (i.e. (0 0 0 1) plane normals) – the so-called twinning product [46,47] in hexagonal Zr. The starting textures, though sample B was slightly more textured than A, did not contain significant basal. It developed, in α, as twinning product [46,47] through the progressive plastic deformations and this was more in sample B. β texture, on the other hand was largely randomized.

3.3. Signatures of relative deformation

Relative deformation was generalized in terms of lattice strain estimates (Fig. 9) and also from experimental data of nano-hardness (Fig. 10) and GAM (Fig. 11). The lattice strain developments in α phase, Fig. 9, has an interesting features – till ≈10% deformation lattice strain developments in sample B was insignificant. This can again be justified from more extensive deformation twinning in sample B. Twinning has shown, in past studies [46,47], to arrest significant developments in lattice strain. It is to be noted that beyond 10% deformation, when contributions from deformation twinning reduced, lattice strain developments between the samples were nearly identical.

The nanoindentation measurements, though extremely effective in putting a clear demarcation between the initial microstructures, had 'limitations' in precise identification of deformed β, especially in case of highly fragmented deformed β in sample B. In spite of such limitations and a large scatter in experimental nano-hardness values (unavoidable – as the degree of plastic deformation is expected to differ between different grains and also between different parts of the same grain), two clear inferences can be drawn. β in sample A remained harder (at least up to ≈5% cold work) – see Fig. 10; though estimated hardness difference in α phase, between the two samples, was marginal at best. The latter confusion is cleared with estimates of in-grain misorientation developments. Harder β and softer α, both in sample A, respectively had lower and higher GAM developments – Fig. 11.

4. Discussions

The present study brings out clear differences in deformed microstructure developments between samples A and B. Such differences can be attributed to the differences between the

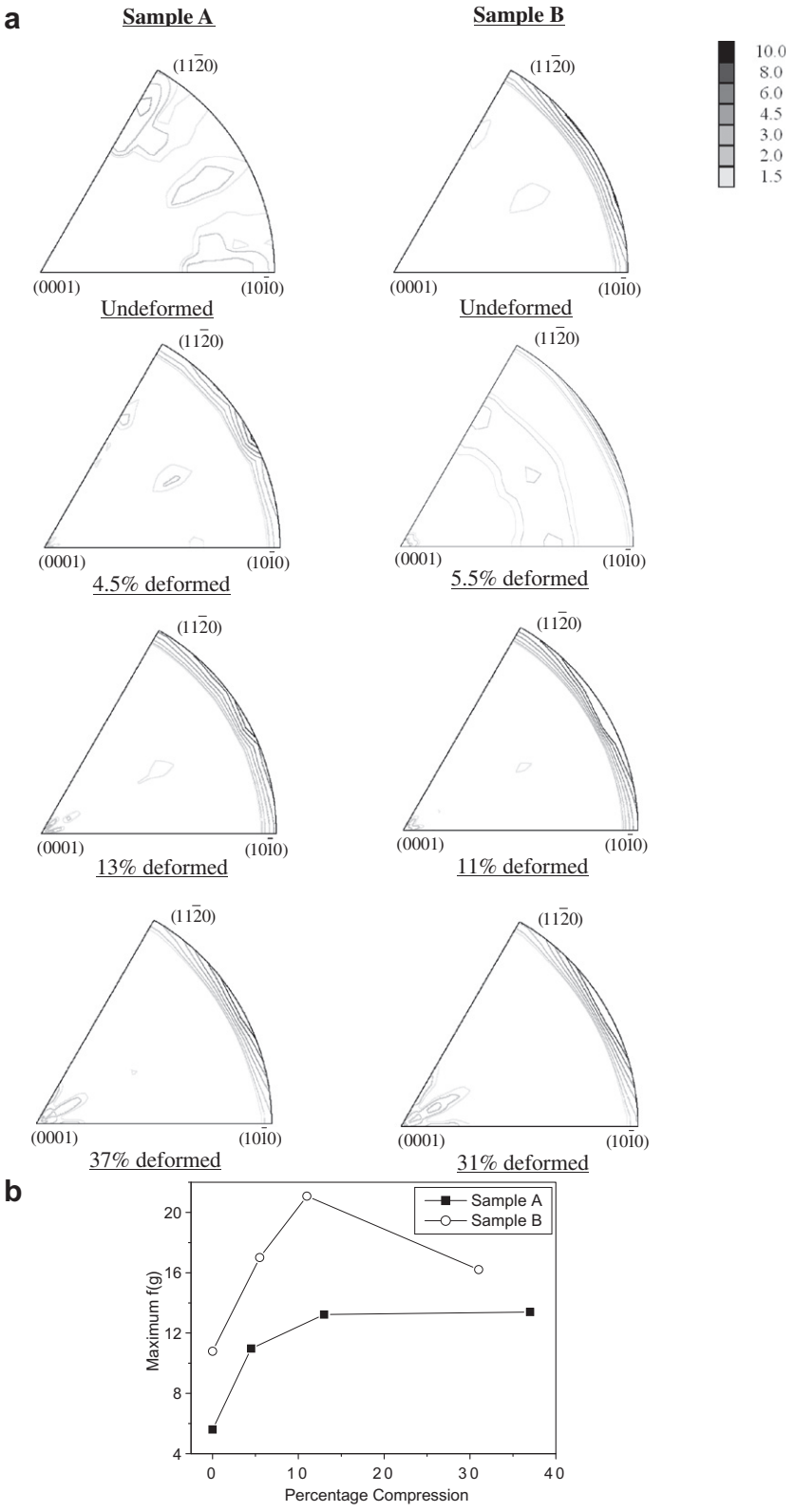

Fig. 7. (a) Texture developments, represented by ⟨0 0 0 1⟩ IPFs, in α phase at different deformations. Measurements were obtained through X-ray diffraction. (b) Maximum *f*(g), or IPF intensity, values as in (a).

starting microstructures, of the respective samples, and resultant differences in strain partitioning and deformation modes. The starting microstructures differed in the grain size of the primary phase (α of sample B was approximately 1.5 times larger) and relative hardness of the second phase (β of sample A was more than two times harder). These, especially the last factor, resulted in significant differences in deformed microstructure developments – rationalized/discussed in the present section.

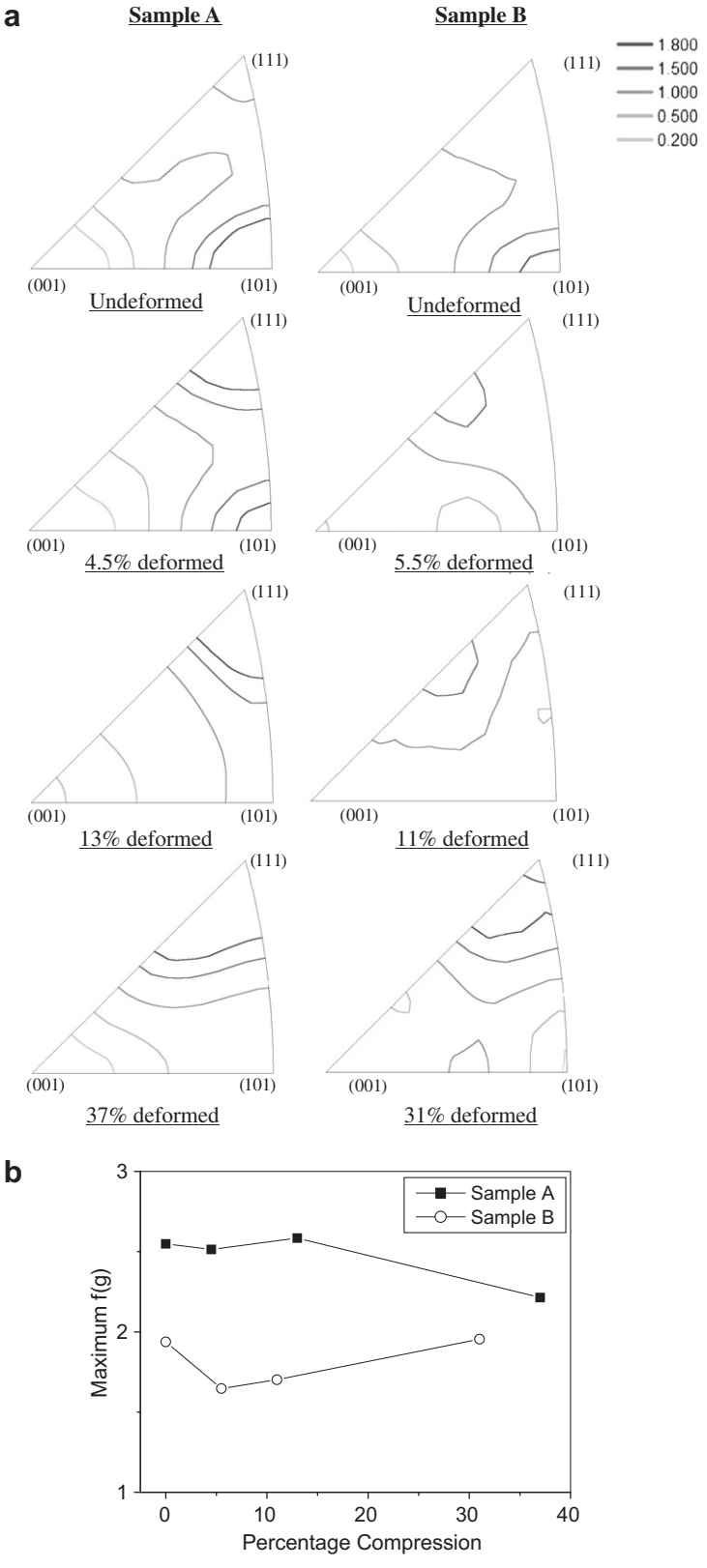

Fig. 8. (a) Texture developments, represented by ⟨0 0 1⟩ IPFs, in β phase at different deformations. Measurements were obtained through EBSD. (b) Maximum *f*(g) or IPF intensity, values of different deformations in (a).

4.1. Strain partitioning

It is expected that the softer phase would accommodate a larger share of the total strain [7,10,31]. Pictorial description of deformed microstructure developments, especially for deformed β – see Fig. 4, is in agreement with such expectation. In sample B the softer β phase was more fragmented, Fig. 5a, and had stronger developments of in-grain misorientation, Fig. 11b. Though this part of

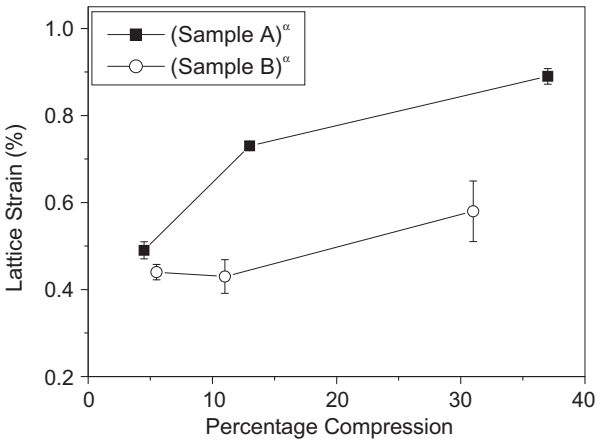

Fig. 9. Lattice strain developments in α phase at different deformations respectively for samples A and B. Standard deviation values in (a) represent the relative linear fit of the Williamson and Hall plots [35–37].

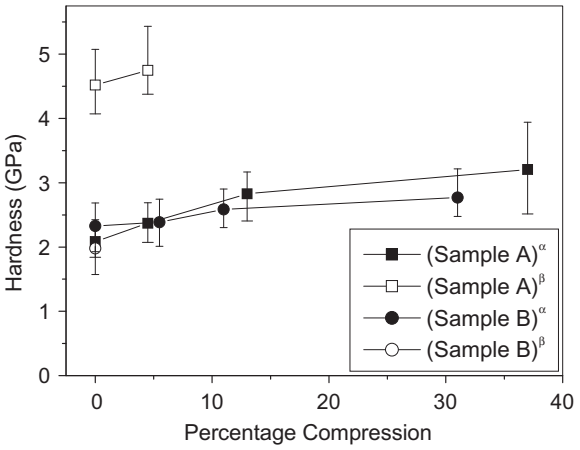

Fig. 10. Nano-hardness values of α and β phases in both samples at different deformations. In sample A, and at the early deformation stages, hardness of deformed β could be estimated reliably. In sample B, on the other hand, fragmented deformed β made conclusive measurements impractical/unreliable. Error bars represent the standard deviation estimated from multiple measurements.

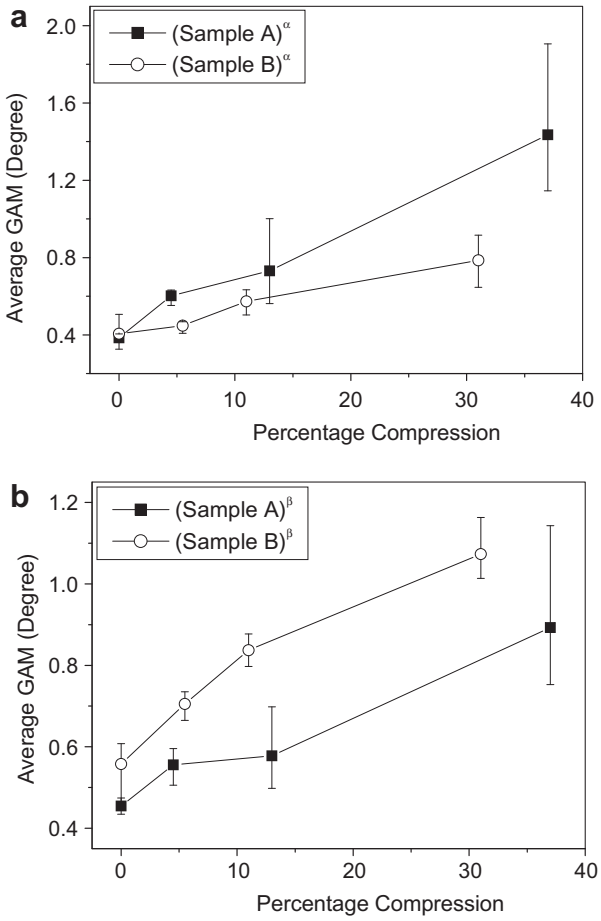

Fig. 11. GAM developments in (a) α and (b) β phases of samples A and B. Error bars represent the standard deviation estimated from multiple measurements.

the results is along the expected lines, effects of such strain partitioning were less apparent on the α microstructure developments. Softer α of sample A developed more in-grain misorientation (Fig. 11a) and lattice strain (Fig. 9) through plastic deformation; but it also had lower fragmentation (Fig. 5b) and weaker developments in deformation texture (Fig. 7). The last two points cannot be justified through strain partitioning alone. Another interesting issue is the deformation texture developments of the β phase, albeit by relatively limited EBSD statistics. In both samples the β texture was randomized – irrespective of the differences in strain partitioning and possible constraints by the surrounding α.

4.2. Deformation twinning

Deformation twinning, observed only in the α phase, was more in sample B. This can be explained in terms of larger grain size and/or presence of softer second phase. Larger grain size is expected [48–50] to promote deformation twinning, though recent studies on twinning in single phase Zircaloy 2 [46,47] showed that $\{10\bar{1}2\}\langle\bar{1}011\rangle$ tensile twins are affected more by crystallographic orientation than by moderate (similar as in the case of the present study) differences in-grain size. Twinning is also expected if slip is restricted [47,51,52]. In sample B, with softer β surrounding the matrix grains, the strain and hence the slip are expected to be restricted/limited in the α phase; while in sample A harder second phase may cause less restrictions. Though difficult to prove conclusively, the patterns of GAM developments, Fig. 11a, and the extent of deformation twinning in the respective samples, Fig. 6, justify such an argument. More extensive twinning in sample B is reflected in the higher fragmentation of the α grains and in stronger developments in deformation texture. The latter was primarily in terms of increased concentration of basal pole, a product of deformation twinning [46,47].

5. Conclusions

The present study involved uniaxial cold compression of two samples –sample A and sample B. Both had a microstructure of hcp α grains with grain boundary and tri-junction bcc β. The two structures, however, had distinct differences: (*i*) α grain size was approximately 1.5 times more in sample B and (ii) β was two times harder in sample A. (ii) was due to fine ω precipitates present in the β phase of sample A. Plastic deformation, in these two samples, had clear differences in microstructural developments. These are summarized below:

- Softer β in sample B had more fragmentation and stronger developments in GAM (grain average misorientation). Similarly, softer α in sample A had more lattice strain and GAM. Such

trends can be justified from the expected patterns of strain partitioning – more strain partitioning being expected in the softer phase.

- Only $\{10\bar{1}2\}\langle\bar{1}011\rangle$ type of tensile twins was observed in α grains of both samples. The amount of twinning was more in sample B. Correspondingly, the α grain size refinement and degree of 'texturing' in sample B was more.
- More extensive twinning in sample B can be justified due to larger grain size and/or softer second phase. Though larger grains, in general, are expected to promote deformation twinning, recent studies in single phase Zircaloy 2 had shown that $\{10\bar{1}2\}\langle\bar{1}011\rangle$ type of tensile twins are affected more by crystallographic orientations than by moderate differences (similar to the present study) in-grain size. Presence of soft β in sample B is expected to restrict strain partitioning and slip. This, on the other hand, does provide an explanation for the more extensive deformation twinning observed in sample B.

Acknowledgements

The authors would like to acknowledge financial support from BRNS (Board of Research on Nuclear Science) and the texture/microtexture measurements at the National Facility of Texture and OIM (a DST-IRPHA facility) at IIT Bombay.

References

[1] B. Karlsson, B.O. Sundstrom, Mater. Sci. Eng. 16 (1974) 161.
[2] M.F. Ashby, Phil. Mag 21 (1970) 399.
[3] Ch. Hartig, H. Mecking, Comput. Mater. Sci. 32 (2005) 370.
[4] Z. Jiang, Z. Guan, J. Lian, Mater. Sci. Eng. A 190 (1995) 55.
[5] T. Takasugi, N. Fat-Halla, O. Izumi, Acta Metall. 26 (1978) 1453.
[6] H.J. Bunge, W. Bocker, Texture. Microstruct. 22 (1993) 29.
[7] L.B. Zuev, V.I. Danilov, T.M. Poletika, S.A. Barannikova, Int. J. Plasticity 20 (2004) 1227.
[8] R.A. Kot, B.M. Bramfitt, Fundamentals of Dual Phase Steels, AIME, New York, 1981.
[9] A.B. Li, L.J. Huang, Q.Y. Meng, L. Geng, X.P. Cui, Mater. Des. 30 (2009) 1625.
[10] M. Kiran Kumar, I. Samajdar, N. Venkatramani, G.K. Dey, R. Tewari, D. Srivastava, S. Banerjee, Acta Mater. 51 (2003) 625.
[11] F.J. Humphreys, M. Hatherly, Recrystallization and Related Annealing Phenomena, Elsevier, UK, 1995.
[12] S. Raveendra, S. Mishra, K.V. Mani, H. Weiland, I. Samajdar, Metall. Trans. 39A (2008) 2760.
[13] B. Verlinden, J. Driver, I. Samajdar, R.D. Doherty, Thermo-Mechanical Processing of Metallic Materials, Pergamon materials series, Cambridge, UK, 2007.
[14] P. Van Houtte, Acta Metall. Mater. 43 (7) (1995) 2859.
[15] B. Verlinden, J. Driver, I. Samajdar, R.D. Doherty, Thermo-Mechanical Processing of Metallic Materials, Pergamon materials series, Cambridge,UK, 2007.
[16] S. Banerjee, P. Mukhopadhyay, Phase Transformations: Examples from Titanium and Zirconium Alloys, First ed., Elsevier Science, 2007.
[17] D. Srivastava: PhD. thesis, Indian Institute of Science Bangalore, 1997.
[18] G.J.C. Carpenter, Can. Metall. Quart 24 (1985) 251.
[19] R.F. Heheman, Can. Metall. Quart 11 (1972) 201.
[20] E.S.K. Menon, S. Banerjee, R. Krishnan, Metall. Trans. A 9 (1978) 1213.
[21] S. Banerjee, Martensitic Transformation in Zr alloys, PhD thesis, Indian Institute of Technology, Kharagpur, India, 1973.
[22] S. Banerjee, R. Krishnan, Metall. Trans. A 4 (1973) 1811.
[23] S. Banerjee, R. Krishnan, Acta Metall. 19 (1971) 1317.
[24] S. Banerjee, G.K. Dey, D. Srivastava, S. Ranganathan, Metall. Mater. Trans. 28A (1997) 2201.
[25] R. Tewari, D. Srivastava, G.K. Dey, J.K. Chakravarty, S. Banerjee, J. Nucl. Mater. 383 (2008) 153.
[26] D.L. Douglass, The Metallurgy of Zirconium, Internal Atomic Energy Agency, Vienna, 1971.
[27] B.A. Cheadle, Zirconium in Nuclear Industry, ASTM STP 633, A.L. Lowe, Jr., G.W. Parry, Eds., ASTM, Philadelphia, PA, 1977, p. 457.
[28] C. Ganguly, in: Proceedings of the symposium zirconium-2002′, BARC, Mumbai, 2002, p. 1.
[29] V.D. Hiwarkar, S.K. Sahoo, I. Samajdar, K. Narasimhan, K.V. ManiKrishna, G.K. Dey, D. Srivastav, R. Tewari, S. Banerjee, J. Nucl. Mater. 384 (2008) 30.
[30] V.D. Hiwarkar, S.K. Sahoo, K.V. ManiKrishna, I. Samajdar, G.K. Dey, D. Srivastav, R. Tewari, S. Banerjee, R.D. Doherty, Acta Mater. 57 (2009) 5812.
[31] S. Cai, M.R. Daymond, R.A. Holt, M.A. Gharghouri, E.C. Oliver, Mater. Sci. Eng. A 501 (2009) 166.
[32] K.Pawlik, P.Ozga, LaboTex, The Texture Analysis Software, Göttinger Arbeiten zur Geologie und Paläontologie, SB4, 1999.
[33] H.J. Bunge, Texture Analysis in Materials Science–Mathematical Methods, Butterworths, London, 1982.
[34] V. Randel, O. Engler, Introduction to Texture Analysis, Macrotexture, Microtexture and Orientation Mapping, Gordon and Breach Science Publishers, Australia, 2000.
[35] B.D. Cullity, Elements of X-ray Diffraction, second ed., Addision-Wesley Publishing, 1978.
[36] C. Suryanarayana, M. Grant Norton, X-ray Diffraction–a Practical Approach, Plenum Press, London, 1998.
[37] G.K. Williamson, W.H. Hall, Acta Metall. 1 (1953) 22.
[38] A.C. Fischer-Cripps, Nanoindentation, Springer, New York, 2002.
[39] W.C. Oliver, G.M. Pharr, J. Mater. Res. 7 (6) (1992) 1564.
[40] T.A. Mason, J.F. Bingert, G.C. Kaschner, S.I. Wright, R.J. Larsen, Metall. Mater. Trans. A 33A (2002) 949.
[41] J.F. Bingert, T.A. Mason, G.C. Kaschner, P.J. Maudlin, G.T. Gray III, Metall. Mater. Trans. A 33A (2002) 955.
[42] A.J. Schwartz, M. Kumar, B.L. Adams, Electron Backscatter Diffraction in Materials Science, Kluwer Academic/Plenum, New York, 2000.
[43] A.H. Cottrell, The Mechanical Properties of Matter, Wiley, New York, 1964.
[44] M.F. Ashby, Strengthening Mechanisms in Crystals, in: A. Kelly, R.B. Nicholson (Eds.), Elsevier, Amsterdam, 1971. 137.
[45] J.W. Christian, S. Mahajan, Prog. Mater. Sci. 39 (1995) 1.
[46] S.K. Sahoo, V.D. Hiwarkar, I. Samajdar, P. Pant, G.K. Dey, D. Srivastav, R. Tewari, S. Banerjee, Mater. Sci. Tech. 26 (1) (2010) 104.
[47] S.K. Sahoo, V.D. Hiwarkar, A. Majumdar, I. Samajdar, P. Pant, G.K. Dey, D. Srivastav, R. Tewari, S. Banerjee, Mater. Sci. Eng. A 518 (2009) 47.
[48] E. El-Danaf, S.R. Kalinindi, R.D. Doherty, Mater. Trans. A 30 (1999) 1223.
[49] G.C. Kaschner, G.T. Gray III, Mater. Trans. A 31 (2000) 1997.
[50] S. Mishra, K. Narasimhan, I. Samajdar, Mater. Sci. Technol. 23 (9) (2007) 1118.
[51] G.E. Dieter, Mechanical Metallurgy, McGraw-Hill Book Company, London, 1988.
[52] E. Tenckhoff, Deformation Mechanisms, Texture, and Anisotropy in Zirconium and Zircaloy, ASTM, Philadelphia, PA, 1988.